Journal of Pharmaceutical Innovation (2025) 20:153
https://doi.org/10.1007/s12247-025-10037-0

RESEARCH

Forced Gas Convection for Uniform Freezing of Lyophilization Vials

Steven J. Burcat[1] · Rohan P. Kadambi[2] · Lorenzo Stratta[3] · Richard D. Braatz[2] · Roberto Pisano[3] · Alexander H. Slocum[1] · Bernhardt L. Trout[2]

Accepted: 28 June 2025

Abstract

Purpose Conventional shelf-freezing in pharmaceutical lyophilization suffers from batch variation and is potentially incompatible with emerging continuous lyophilization systems. This work presents a forced gas convective freezing chamber for suspended vials in cross-flow to improve the quality of the freezing process and meet the continuous lyophilization needs.

Methods First, computational fluid dynamics simulations were performed to determine key process parameters. Then, physical chambers were built to meet these requirements. Sets of twenty 10R vials containing 3 mL of aqueous solution were frozen to characterize the per-vial heat transfer. Additionally, a novel nucleation technique was investigated where conditioned vials were exposed to an impulse of $<-30°C$ gas. Finally, frozen vials were completely dried in 12 h in an attached vacuum chamber.

Results The chambers conditioned vials from 25°C to −1°C in under 20 min, with final vial temperatures varying by less than 0.5°C. The impulse technique induced nucleation in all vials within 30 s without significantly cooling them. After nucleation, the system accessed slow (0.05 g/min) and rapid (1.0 g/min) solidification rates, as well as post-solidification procedures including typical ramp and hold protocols. Dried vials had residual moisture below 2.5 wt% and showed no signs of collapse.

Conclusions This freezing chamber was demonstrated to track gas temperature setpoints as low as −50°C within ±1°C and induce nucleation in all vials virtually simultaneously, enabling excellent control of the freezing process. The chamber's cooling via forced convection and its available front and back faces make it compatible with integration into a continuous lyophilization system.

Keywords Lyophilization · Freezing · Nucleation · CFD · Continuous manufacturing

Introduction

Lyophilization (vacuum freeze drying) is a technique that is used to stabilize pharmaceutical products for storage and transportation [1]. Typically, the product solution is filled into vials that are placed on temperature-controlled shelves in a chamber capable of pulling a vacuum below 20 Pa. This process removes almost all water from aqueous formulations in three steps. First, the product is frozen by cooling the vials to low temperatures, typically below −30°C. Then a vacuum pump is activated, and the vials are gently heated to drive sublimation of the bulk water in a process called primary drying. Once all the bulk water in the vials has been removed, additional heat is applied to drive off the bound water in secondary drying [2]. Overall, these processes are slow, with freezing taking a few hours and the drying processes requiring 1–2 days, even when removing only 3 mL of water from each vial. Most commercial lyophilization is done in large batches, suffering from process nonuniformity and inefficiencies that could be improved by transitioning to continuous manufacturing methods [3, 4].

While freezing only occupies 10% of the total process time, it creates the ice crystals that determine the pore network that controls drying. When ice sublimates from the top of the frozen mass, it leaves behind a complex product structure surrounding an interconnected network of pores formed by the voids previously filled by ice, creating a path through which water vapor liberated from ice lower in the vial must travel [5–7]. Additionally, the size of the ice crystals influences the specific surface area and, consequently, the extent of the ice-water interface, which is one of the factors responsible for the denaturation of certain biomolecules [8, 9]. Lastly, the amount of unbound water and the desorption rate are

Steven J. Burcat and Rohan P. Kadambi are co-first authors.

Extended author information available on the last page of the article

Published online: 29 July 2025

affected by the pore network, which will impact the residual water content in the final product [10].

The freezing process can be divided into several parts: conditioning, where vials are cooled from ambient conditions to just below 0°C; nucleation, where ice crystals begin to form; solidification; where all the liquid water is frozen; and finally quenching, where the vials are lowered to −40°C to prepare for drying [1].

While nucleation is a crucial step that sets the initial ice crystal structure, it is difficult to control due to its stochastic nature [11–13]. Methods to control nucleation generally begin with a conditioning step that brings all vials in a batch to a slightly sub-cooled condition where spontaneous nucleation is unlikely. Then a change is induced to increase the nucleation probability, such as the seeding of crystal with an ice fog technique, the direct cooling of the liquid water with the vacuum-induced surface freezing technique, or the bulk cooling of the system with aggressive temperature ramps [14, 15].

During solidification, the size of the ice crystals grown is inversely related to the solidification rate. Therefore, rapid freezing rates result in a more restricted pore network during drying. Even after complete solidification, some products benefit from the inclusion of an annealing step. During annealing, the vials are raised back to an intermediate temperature to increase ice crystal size through Ostwald ripening or to homogenize the polymorphs of the solid product being lyophilized [16, 17].

At industrial scales, pharmaceutical lyophilization is typically performed in batch sizes ranging from 1,000 to 10,000 vials due to the slow process time. In these machines, vials are cooled conductively through contact with a temperature-controlled shelf on which they sit. The cooling conditions for individual vials often vary significantly across the shelf, and the large shelves have practical limitations on their maximum temperature change rates due to their large thermal mass. This cooling variability leads to highly variable cake structures, resulting in varying drying rates, but the batched nature of the process limits its overall speed to that of the slowest vials [18].

Techniques such as spin freezing address this non-uniformity by both treating each vial individually and coating the product liquid solution across the entire surface area of the vial [19], a process implemented commercially by RheaVita. While spin-freezing can control the rate of solidification after nucleation, it does not control the nucleation time or temperature of the products, and the process of spin-freezing significantly increases the air-water and water-solid interfacial areas [9, 20–23].

Other continuous lyophilization systems without spin freezing, which can control the freezing of several vials at a time to create a balance between uniformity and production rate, have been proposed but have not been realized. Continuous manufacturing techniques can reduce current industrial lyophilization times, eliminate the process inhomogeneity introduced by large batches, and implement model-based closed-loop process control. The control and quality improvements from continuous manufacturing could expand the set of products benefiting from lyophilization, and its scale-up and flexibility benefits can streamline supply chains and allow for rapid production changes when needed. These continuous processes necessarily move vials through the lyophilization system, which makes direct shelf cooling cumbersome due to the generation of particulates from rubbing potentially violating the strict sterility requirements of injectable drug products [3, 4].

This work presents the design, manufacture, and testing of a forced gas convection freezing chamber that can integrate into a continuous lyophilization process. This chamber blows inert gas at a controlled temperature and flow rate across rows of suspended vials that can move through the chamber. While this chamber operates similarly to blast freezers, the use of liquid nitrogen for gas temperature control allows it to be much smaller, improving uniformity between samples. Additionally, the liquid nitrogen source ensures that the recirculating gas is dry nitrogen, removing potential sources of frost from the gas flow [24].

Methods

Both simulation and physical prototyping were used to evaluate a forced convection freezing chamber for vials in cross flow. First, simulations were used to compare potential geometry choices and flow configurations and provide a feasibility study. Physical prototypes were then designed and assembled considering key results from the simulation and practical limitations. Finally, tests were performed with vials to assess the efficacy and uniformity of the freezing process. This study used 10R vials (Soffieria Bertolini, Candiolo, Italy) filled with a 3 mL solution of 5 wt% mannitol (Sigma-Aldrich) dissolved in water (Milli-Q) and filtered through a 0.2 μm filter as a nominal formulation.

Functional Requirements

The chamber design was evaluated on its ability to satisfy key functional requirements used to guide its design. These functional requirements address the system's cooling mechanism and associated parameters, establishing the criteria to measure the system's success.

1. The chamber must be capable of completing the freezing process in less than 2 h.

2. The vial temperatures in the chamber must be maintained within ±1°C of the desired setpoints at the end of each step in the freezing process.
3. The chamber must be capable of accessing temperature setpoints between −50°C and 10°C.
4. The chamber must trigger a nucleation event via a controlled stimulus.
5. The vials must not directly contact the inner surfaces of the chamber.

Requirement 1 is set to meet or exceed typical cooling rates in existing batch lyophilizers. Requirement 2 is set by the resolution of the thermocouples used to assess the system. Requirement 3 ensures that the chamber can reach temperatures relevant to all parts of the freezing process. Requirement 4 is necessary to reduce variability in drying performance for vials produced by this chamber. Requirement 5 simplifies the integration of this chamber into a continuous lyophilization system.

Simulation

COMSOL MultiPhysics version 5.6 was used to simulate various geometries and configurations relevant to the freezing of lyophilization vials. The vials were modeled as 24 mm diameter glass cylinders with 3 mL of liquid water inside, while the vial stoppers and the tray holding the vials were neglected. The flow around the vials was simulated by solving the Navier–Stokes equations in the continuum regime under laminar flow conditions. Properties for the cooling gas were calculated using COMSOL's built-in values for nitrogen with ideal gas assumptions as relevant. The cooling gas was assumed to have a constant inlet temperature of −5°C unless noted otherwise. Three classes of simulation were performed to analyze this system.

First, a set of simulations was run using simplified geometries and boundary conditions (e.g., no heat flux at the walls) to quickly assess the efficacy of a variety of flow configurations and vial layouts. These more computationally efficient preliminary simulations are necessary to narrow the design space for both detailed simulation and prototype manufacture.

Second, a simulation was run on a practical geometry close to the final as-built chamber design. This simulation included a more complex geometry and more realistic boundary conditions (e.g., free convection on the outside of the walls) to demonstrate that the results from the first set were transferable.

Finally, a set of single-vial simulations was performed to evaluate the theoretical efficacy of a thermal impulse-induced nucleation strategy.

Hardware Design and Characterization

While this chamber underwent several hardware iterations (see Appendix B) to meet the design parameters set from the simulations, this work only presents a detailed description of the final chamber. This chamber is built around a magnetic levitation motion system from Planar Motors Inc. and includes a gas recycle system to improve cooling efficiency. Magnetic levitation and the convective gas flow remove contact between system components, facilitating future GxP operation. The uniformity and stability of the convective gas temperature and flow within the chamber were measured using T-type thermocouples (PerfectPrime TL0024TT) and a hot wire anemometer (VelociCalc Air Velocity Meter 9545).

Gas Temperature Control

This convective gas cooling strategy fundamentally requires a large and stable supply of cold gas to control vial temperature. For this study, boiling liquid nitrogen was injected directly into the flow to generate the appropriate temperatures. This strategy utilizes both the efficiency of the enthalpy of boiling as a cold source and the boiling temperature, 77K, to access cryogenic temperatures.

Despite these benefits, using liquid nitrogen as a cold gas source also carries notable complications. In particular, the cryogenic temperatures can freeze many actuators, the system feed contains an actively boiling two-phase flow, and the liquid nitrogen dewar pressure is not regulated.

The gas temperature is controlled by a cascade controller with a fast inner loop manipulating an inlet feed valve (carbon steel ball valve with a graphite seal) with an electrical actuator (Assured Automation S40170UV19) based on the outlet gas flow rate (Alicat M-2000SLPM-D/CM). The outer control loop sets the flow setpoint for the inner loop based on the current gas temperature. This cascade structure is described in detail in Appendix C.

Freezing Performance Characterization

After validating the hardware used to drive the freezing process, experiments were run for vials with solution in the chambers. The solution temperature in each vial was measured by T-type thermocouples (PerfectPrime TL0024TT) suspended in the center of the solution 2 mm above the bottom of the glass in each vial, with their positions secured

by feedthrough features in a 3D-printed cap held in the vial neck. The vials were suspended from their necks and arrayed on a tray in two rows of five vials each in a 40 mm spaced hexagonal pattern. Each freezing chamber holds two trays of ten vials for a total of 20 vials.

Multiple freezing chambers were manufactured, including versions compatible with load locks [25] to provide physical separation and rapid transition between cooling zones at different gas temperatures.

Nucleation

The gas temperature change for the impulse nucleation technique can be generated in two different ways. When using a single chamber, the impulse is generated by fully opening, then fully closing, the liquid nitrogen feed valve for 30 s. When using multiple chambers, the vials are moved into and out of a chamber at $<-30°C$. Other nucleation methods, such as ice-fog or vacuum induced surface freezing, could be implemented, but they would require additional hardware capability installation, whereas the thermal impulse method utilizes the existing capabilities of the forced convection chambers.

This work uses two methods to measure the distribution of times at which nucleation occurred when using the thermal impulse nucleation strategy. First, the nucleation event is observed directly for multiple vials by replacing one wall of the chamber with an acrylic window. When nucleation occurs, the newly formed ice crystals turn the transparent liquid solution opaque, providing a visual indication. Second, thermocouples placed directly in each vial detect the nucleation event by measuring when the sub-cooled solution temperature jumps to the equilibrium freezing temperature. While thermocouples can affect nucleation behavior by providing sites for heterogeneous nucleation, this effect is not expected to affect this measurement because of rapid homogeneous nucleation that occurs in response to a thermal impulse. This claim is validated in Section Induced Nucleation, where there is no difference in the distribution of nucleation times observed both with and without thermocouples.

Inferred Vial Dynamics

The restrictions from thermocouple wires prevent testing where the vials are moved between chambers operating at different temperature setpoints. This limitation can be overcome by inferring the vial dynamics from the gas temperature when the heat transfer between the two is well characterized. The per-vial data collected in Section Freezing Performance Characterization can be used to estimate the per-vial convective heat transfer coefficient, h. Specifically, the average temperature in the vial during these tests follows

$$\frac{dT_{vial}}{dt} = \frac{hA}{mC_p}\left(T_{vial} - T_{gas}\right) \tag{1}$$

With the true measured dynamics of T_{vial} and T_{gas}, the only unknown parameter in Eq. 1 is h. As described in Appendix D, this value can be fit for each vial using a least squares method, and then those per-vial h values can be used to estimate the dynamics of the system when only the gas temperature is measured.

Lyophilization Performance

Formulations with 3 mL of a 5 wt% mannitol solution typically require 20 h to complete primary drying in laboratory tests. However, batches containing vials with a narrow distribution of larger pores can be dried faster because they can tolerate increased power delivery without exceeding the cake collapse temperature. Studies using induced nucleation strategies to control the freezing process have demonstrated the ability to reduce the primary drying time to 10 h [15].

A lyophilization experiment was performed to show that vials frozen by this system can dry at accelerated rates. First, 20 vials across two trays were frozen using a simple protocol consisting of a 30 min conditioning step where $T_{gas} = -3°C$, an impulse induced nucleation stimulus where $T_{gas} = -45°C$, a 15 min solidification step where $T_{gas} = -3°C$, and finally a 30 min quenching step where $T_{gas} = -45°C$. While this experiment did not include an annealing step, which is common for mannitol-based formulations, the chamber temperature control could easily integrate this process into the freezing protocol, as described in Section Solidification, Freezing, and Annealing. The trays carrying frozen vials were then transferred to a vacuum chamber through a compatible load lock, emulating continuous operation. This vacuum chamber maintained its pressure below 10 Pa throughout the experiment, and the energy for sublimation was supplied to the suspended vials via radiation with the chamber walls. The vials were dried at an average rate of 0.3 g/hr by holding the wall temperature at 30°C so that the 3 mL of solution would complete primary drying in 10 h. After primary drying, the vials remained in the vacuum chamber for an additional two hours to complete secondary drying before being stoppered under vacuum.

The pressure ratio test was used to determine the end of primary drying by detecting a reduction in the moisture content in the vacuum chamber. Specifically, the end of primary drying is the time at which a Pirani pressure gauge (Agilent Varian PCG-750), which is sensitive to moisture, and a capacitive diaphragm gauge (MKS Baratron Type 626), which is not, report the same pressure [26]. The physical appearance of the resultant cakes was assessed, and their final residual

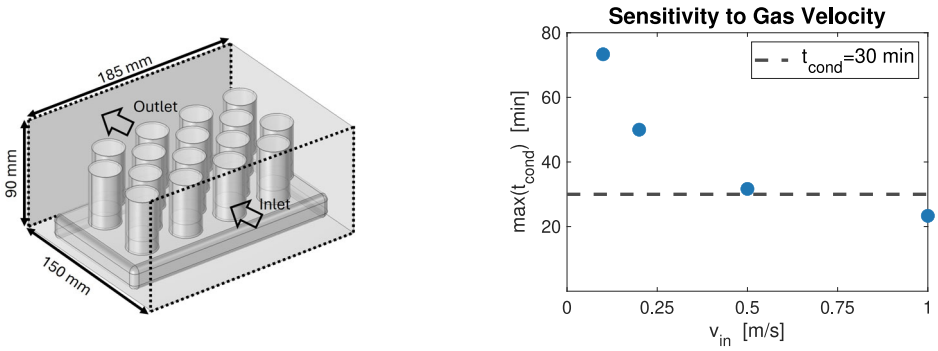

(a) (b)

Fig. 1 (a) The simplified geometry simulated and (b) the sensitivity of this system to the inlet velocity at the nominal inlet and outlet geometries

moisture was measured using Karl Fisher Titration (Metrohm 831 KF Coulometer).

Results and Discussion

Simulation Results

As described in Section Simulation, the objective of the simulations was to identify important geometrical considerations and the relationship between critical process parameters like flow rate and the overall process timescale. The effect on process timescale is summarized by t_{cond}, the time at which the difference between temperature of the water in a vial and the temperature of the gas falls below 1°C. Preliminary simulations used to determine gas port orientations and the vial arrangement are described in Appendix A.

Simplified Geometry Conditioning

The geometry used for the initial simulations is shown in Fig. 1a. This configuration blows cold gas across a loose hexagonal packing of vials with spacing that allows gas to flow between them. To achieve the 2 h total freezing time outlined in Section Functional Requirements, a target of 30 min was placed on the slowest t_{cond} for the simulation. Figure 1b shows that gas flow rates above 0.5 m/s are required to achieve this target.

The simulation setup in Fig. 1a also provides detailed vector fields for the gas velocity within the chamber. Figure 2a shows that after impinging on the first row of vials, much of the cold gas deflects upwards and flows over the vials to the outlet. Restricting the outlet to a 10 mm gap below the vials encouraged flow through the array, as shown in Fig. 2b. Adjusting the outlet reduced the t_{cond} for the slowest vial in the simulation from 32 to 25 min at a gas velocity of 0.5 m/s.

An analogous study was conducted by varying the inlet geometry of the system. Representative results for an inlet velocity of 1 m/s are shown in Fig. 3. The conditioning time of the slowest vials in the back row was not sensitive to the inlet geometry, despite small improvements in the t_{cond} for vials in the front row when shrinking the inlet height. Because the system is limited by the slowest cooling vials, it is not sensitive to the inlet geometry.

Complete Geometry Conditioning

The simple geometry results were used to set the inlet gas velocity and the inlet and outlet geometries for a more realistic simulation. This simulation is based on a chamber design with two inlets on opposite side walls and a central outlet channel. The chamber is sized around a Planar Motors fly-

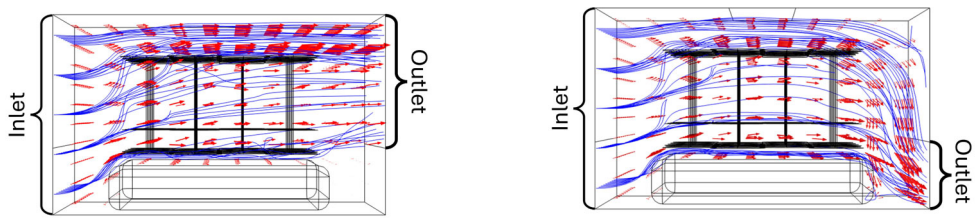

(a) (b)

Fig. 2 The flow fields for the (a) full and (b) restricted outlet geometries. The relatively larger vector magnitude above the vials in the full outlet condition is indicative of gas skipping over the vials

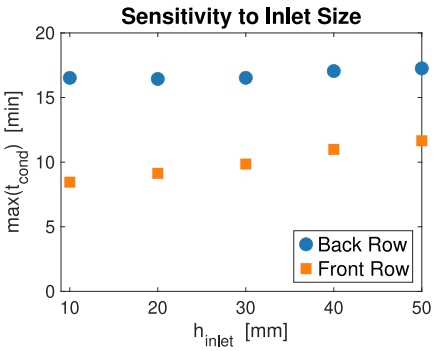

Fig. 3 The sensitivity of conditioning time for first row vials and last row vials to restricting the inlet geometry

way with an angled wall to interface with a load lock and a tray carrying three rows of vials on each side. The geometry of this simulation, shown in Fig. 4a, uses a symmetry plane through the outlet channel and a heat flux boundary condition of 20 W/(m^{2}K) on the external walls to mimic free convection conditions.

The results of this simulation with an inlet gas velocity of 1 m/s are shown in Fig. 4b. At the given conditions, the conditioning time across the rows of vials clearly varies, with the first, second, and third rows taking 30, 38, and 50 min respectively. This trend is consistent with the results from the simplified simulations, with the back row cooling most slowly, but with slightly slower t_{cond} values overall. While including more rows of vials increases productivity, using fewer rows reduces the variation in temperature across the vials, improving the system's robustness to disturbances in the gas temperature. Given these considerations, the hardware prototype described in Section Physical Prototype Design and Validation uses two rows of five vials per side of the chamber to balance uniformity and productivity.

Single-Vial Impulse Nucleation

Rapidly cooling a small volume of water within the vial can significantly increase its likelihood of nucleating without changing the average water temperature. A set of single-vial simulations evaluated the effects of using a step change in the cooling gas temperature to achieve this localized nucleation. This fast temperature change is made possible in the physical chamber by the convective cooling and the use of liquid nitrogen as a cold source, and it is not possible in traditional lyophilizers.

Figure 5a shows a cross section of the geometry used in these simulations. In these simulations, all temperatures were assumed to start at the conditioning temperature, and the system response to step changes in the gas temperature was analyzed. Figure 5b shows that local subcooling of around 15°C can be induced in the vial before the bulk vial temperature drops by 1°C. While larger impulses increase the local subcooling, and therefore the probability of nucleation, this effect has diminishing returns.

Physical Prototype Design and Validation

The freezing chamber, shown in Fig. 6, incorporates the findings from the simulation results. Wide inlets on opposite sides of the chamber and a restricted central outlet channel direct gas across two rows of vials. Most of the gas exiting the chamber through the outlet channel is recirculated through the chamber using a diffuser and C-shaped recirculation ducts. The front and rear faces can be covered by plates to operate the chamber independently, or multiple chambers can be connected to each other or load locks to create an integrated system. The freezing chamber can produce inlet gas velocities upwards of 1 m/s and access the −50°C to 10°C range of temperatures from Section Functional Requirements. While

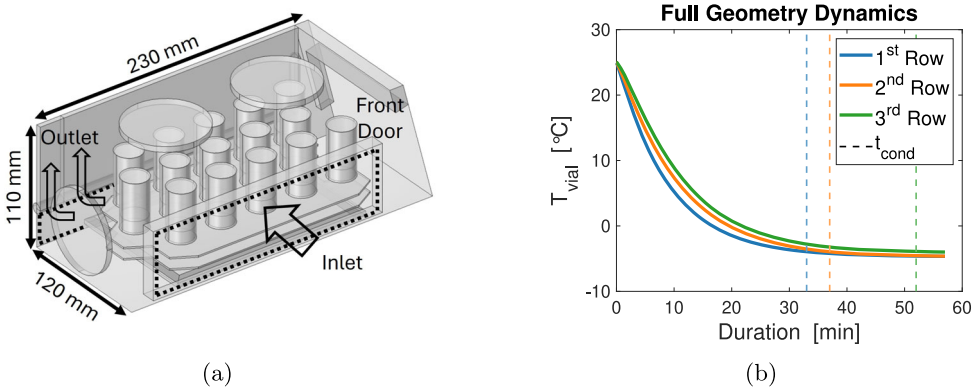

Fig. 4 (a) The geometry simulated to match the freezing chambers. (b) The maximum vial temperature in each row

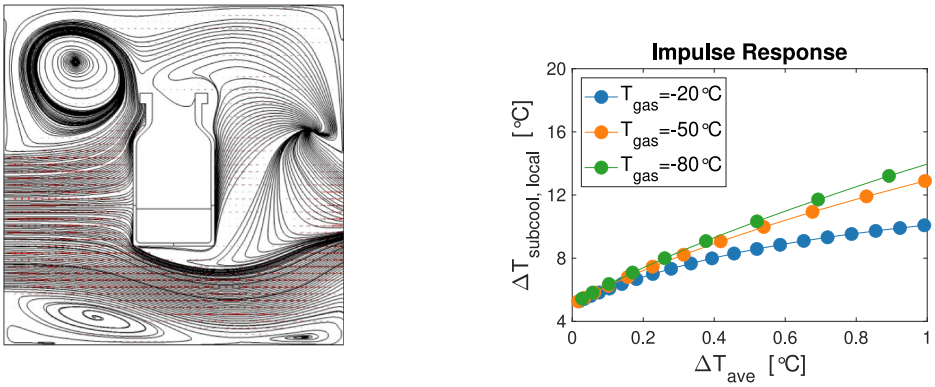

Fig. 5 (a) Typical flow field of the geometry simulated. (b) The degree of subcooling at the front face of the vial over the time that it takes bulk vial temperatures to decrease by 1°C. This process takes 80, 50, and 40 s at the −20°C, −50°C, and −80°C conditions, respectively. The temporal spacing of each marker is 3 s

this chamber was not operated in a GxP-compliant manner, it is reasonable that such a system could be achieved through filtration of both the recirculating gas flow and the liquid nitrogen fresh feed.

The chamber was cast (Yankee Casting in Enfield, CT) and machined (Startsomething LLC in Somerville, MA), while the recirculation ducts and diffuser were manufactured by welding bent and rolled sheets (Startsomething LLC in Somerville, MA). These components were all fabricated from aluminum for its machinability and to remove the risk of differential thermal strain creating loads at the component interfaces. A fresh feed of liquid nitrogen is injected at the top of the recirculation ducts, where it mixes with the recirculated gas along the vertical length before the evaporated nitrogen is blown across the vials by muffin fans (Delta FFB0448EN-00EEY). A set of these fans also draws the cooling gas out of the chamber through the central outlet, preventing backflow. Using muffin fans directly in the flow reduces the duct size, and the heat generated from ohmic losses keeps the fans from freezing. These muffin fans have sealed bearings, protecting the gas flow from contamination.

Gas Recirculation

The gas recirculation system, consisting of two recirculation ducts and one diffuser, reduces nitrogen consumption and buffers the temperature difference between the fresh feed liquid nitrogen at 77K and the target gas temperatures.

The recirculation ducts, shown in Fig. 7a, guide the recycled gas flow from the diffuser back into the freezing

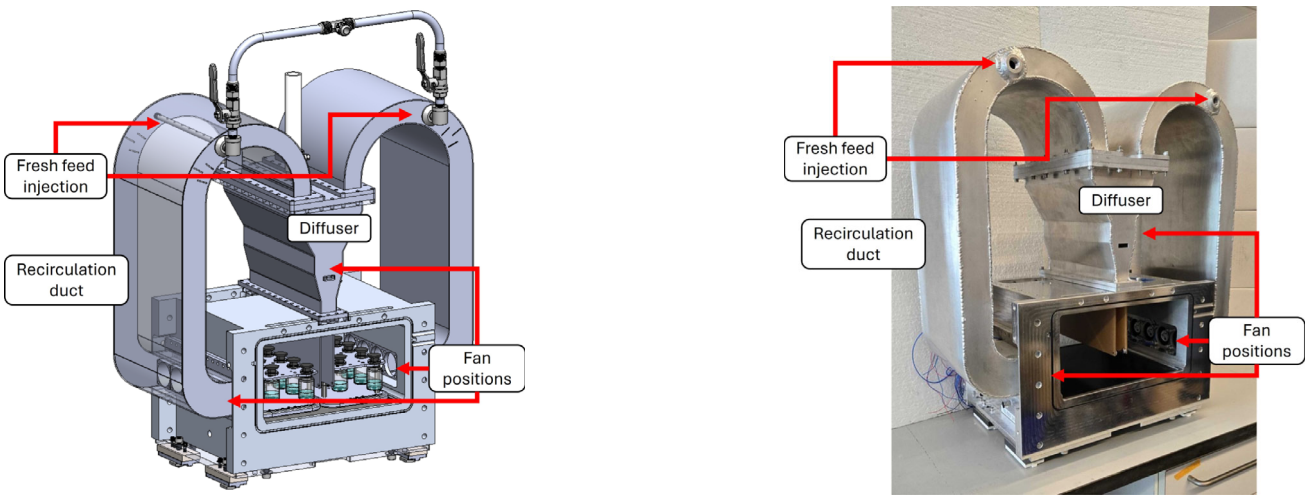

Fig. 6 Comparison of the (a) CAD and (b) as-built freezing chambers

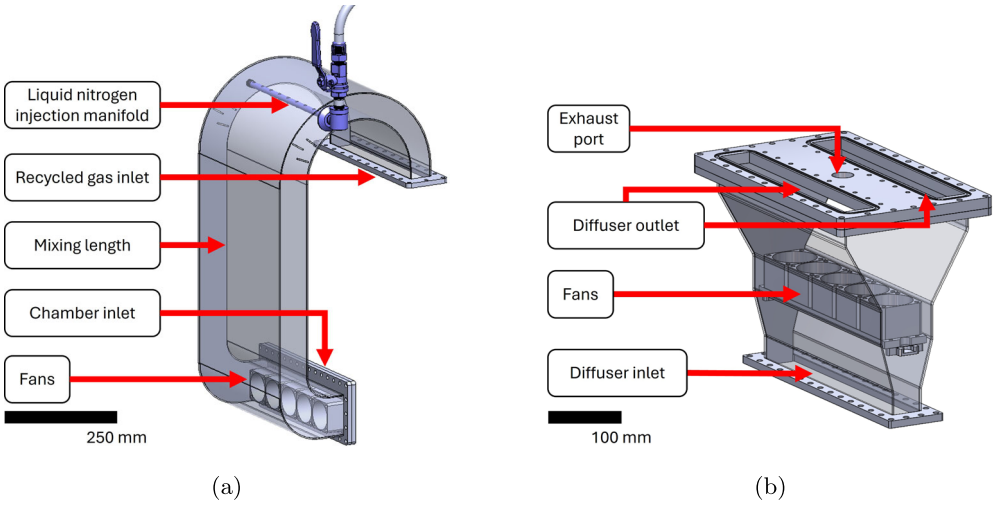

Fig. 7 The freezing chamber uses recirculation ductwork consisting of (a) two recirculation ducts and (b) one diffuser to conserve gas and energy usage while cooling vials

chamber. Fans at the bottom of the recirculation ducts pull gas through the duct and push it into the chamber to cool the vials. The recirculation duct is bolted to the side of the chamber and the diffuser with O-ring seals, allowing it to be removed for maintenance.

The liquid nitrogen feed is injected into the top of the recirculation ducts through a manifold that spreads the liquid nitrogen feed across the width of the recirculation duct to improve the temperature uniformity across the duct. This distribution allows the duct's mixing length to be shortened because the gas only needs to mix across the duct's height, which is much smaller than its width. Using liquid nitrogen to cool the nitrogen gas flow allows for a direct injection of the cooling fluid, enabling the chamber to utilize both nitrogen's heat of vaporization and its sensible heat.

The diffuser shown in Fig. 7b splits the gas flow from the chamber outlet to feed the recirculation ducts. Fans are located within the diffuser to pull gas out of the chamber. The diffuser's exhaust port allows gas to exit the freezing chamber, compensating for the mass entering the system through the liquid nitrogen injection manifolds.

Gas Uniformity

Driving uniform vial cooling requires the system to maintain uniform flow rates and temperatures across the chamber. While the simulation simply assumes inlet gas parameter uniformity, this condition must be verified in situ. The liquid nitrogen manifold, recirculation duct mixing length, and muffin fans provide strong mixing of the recycle gas and the fresh liquid nitrogen feed to generate the inlet velocity and temperature profile shown in Fig. 8. The oscillation in the velocity data (Fig. 8a) corresponds to the measurement crossing the centers of and areas between fans.

Although the sides of the chamber mirror each other, they are not guaranteed to operate at the same temperature. The liquid nitrogen flow is sensitive to differences in flow resistance that arise from typical manufacturing vari-

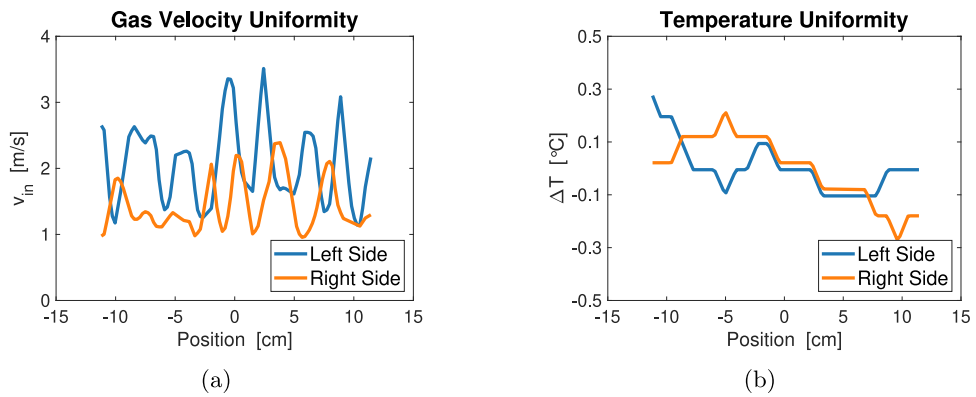

Fig. 8 The freezing chamber achieves excellent (a) velocity and (b) temperature uniformity across the inlet faces

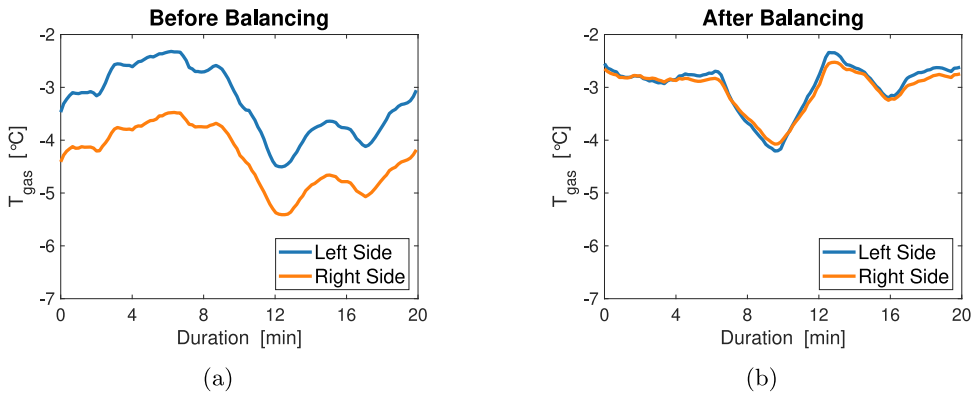

Fig. 9 Side-to-side temperature difference (a) before and (b) after side balancing

ance and upstream piping geometry. Manual balancing valves upstream of the injection manifolds allow an operator to adjust the relative restriction between the two sides of the chamber to flow an equal amount of liquid nitrogen, resulting in the balanced cooling conditions shown in Fig. 9.

The hardware design addresses the spatial uniformity of this chamber, but the temporal variation in the gas temperature requires the active control described in Section Gas Temperature Control. Boiling liquid nitrogen in the feed line creates significant flow instabilities and pressure variations, changing the fresh feed flow rate required to maintain a constant temperature. Figure 10 shows how the implemented control system stabilizes the gas parameters within the chamber, enabling consistent freezing to occur.

Freezing Performance

The use of per-vial thermocouples in the freezing chamber enables detailed monitoring of the vial temperature variation.

Conditioning

The results of the conditioning experiment reported in Fig. 11 show that the conditioning time is about 12 min for the front row and 13 min for the back row. These values are both closer to each other and lower than those predicted by the simulation, likely because the gas flow rate in the chamber exceeds the simulated values. The vial temperature oscillation after initially reaching the conditioning temperature results from the stabilization of the gas temperature by the control system described in Section Gas Temperature Control. This cooling rate and uniformity meet the system requirements outlined in Section Functional Requirements.

Induced Nucleation

The results from the thermal quench nucleation testing with thermocouple measurement, reported in Fig. 12, show that the vials nucleate within 15 s of each other, and the temperature variation between vials at their nucleation event is less than 1°C. Optical nucleation observations found a similar 20 s nucleation window (Fig. 13), indicating that the presence of the thermocouple does not significantly affect the nucleation process process under these conditions. Thus, the measured nucleation temperature distribution during system characterization is expected to be representative of chamber operation, when vial temperature is not directly measured with thermocouples. While it is possible that this nucle-

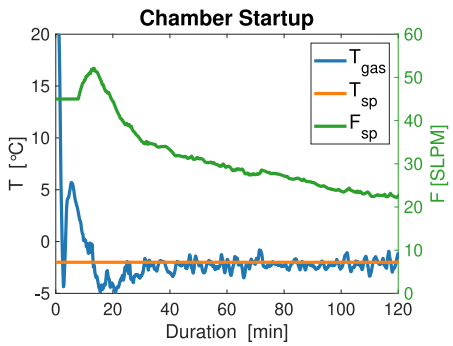

Fig. 10 The required flow rate to maintain a constant temperature set-point changes during operation

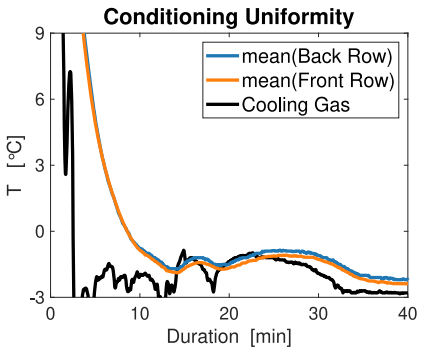

Fig. 11 Empirical conditioning time data collected inside the freezing chamber

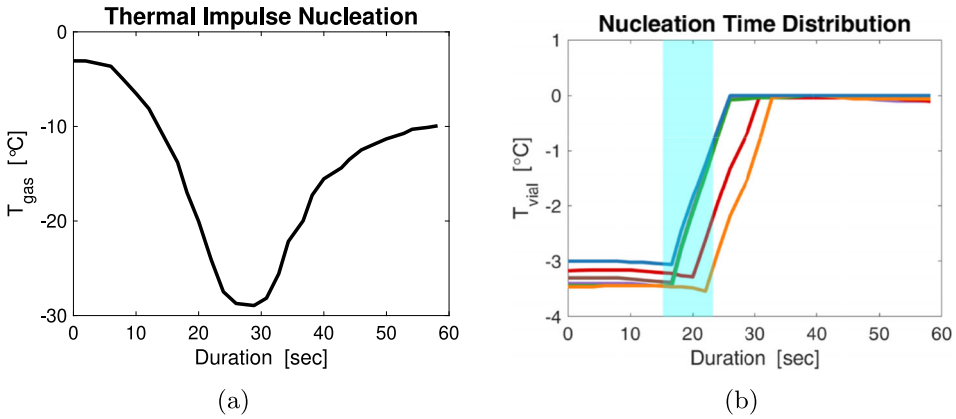

(a) (b)

Fig. 12 When conditioned vials were exposed to the rapid change in gas temperature in (a), they all nucleated within 15 s of each other and at temperatures varying by less than 1°C (b)

ation event is induced in some vials by water vapor in the vial headspace crystallizing and falling into the solution, the video in ESM01 shows that the nucleation front starts from the bottom of multiple vials, which would not be possible with ice fog.

Solidification, Freezing, and Annealing

As described in Section Inferred Vial Dynamics, the temperature trajectories collected in Fig. 11 can be used to fit a convective heat transfer coefficient for each vial. This single parameter fitting strategy accurately reproduces the measured data in Fig. 14b. Figure 14a shows the range in fit parameters across vials in the chamber, indicating nearly a 30% difference between the most extreme vial cooling rates.

Estimation of these coefficients allows inference of the dynamics, controllability, and uniformity of the post-nucleation processes in this chamber. Solidification is likely to be the slowest process because water has a large heat of fusion and only about 1% of the water solidifies during the short nucleation event. This process step is most sensitive to variation in h, as the ice crystal growth rate and corresponding crystal size distribution is sensitive to both the rate of energy removal and the temperature. As shown in Fig. 15, this chamber can access both rapid, <5 min, and slow, >30 min, solidification by changing the convective gas temperature.

After solidification, various freezing protocols can be accessed as shown in Fig. 16. This chamber can achieve the typical 1°C/min ramp rates used in batch lyophilizers, immediate quenching down to −40°C, or more complex protocols including an intermediate annealing step.

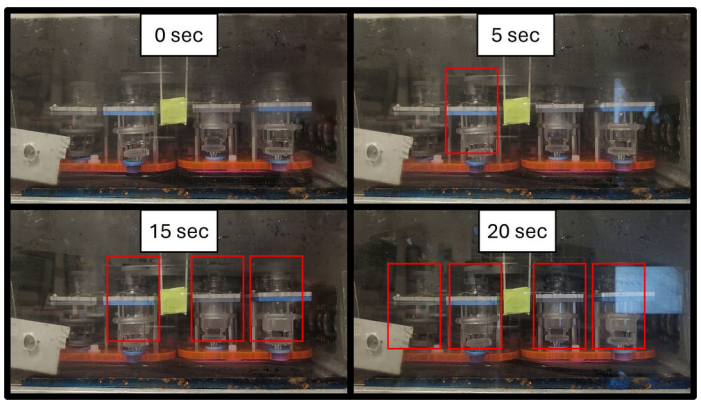

Fig. 13 The efficacy of impulse nucleation can be observed optically. In each frame (timed after the impulse nucleation began), nucleation is identified by the liquid becoming opaque from the ice crystals and is highlighted with red rectangles

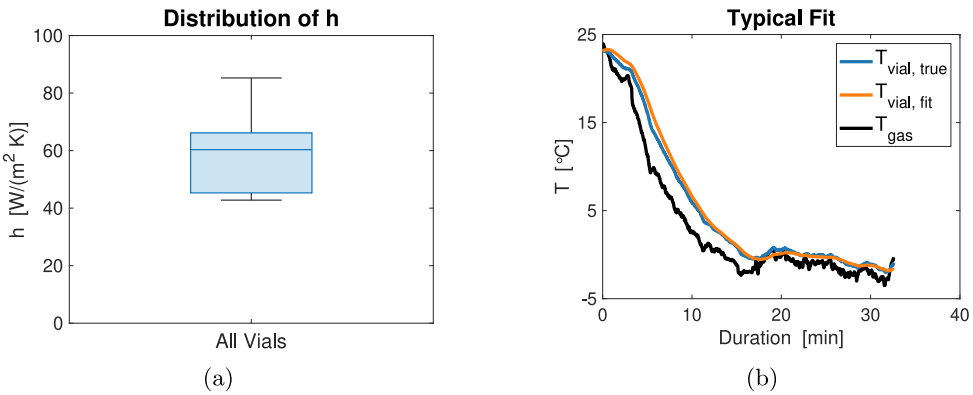

Fig. 14 (a) The distribution of convective heat transfer coefficients found by fitting the thermocouple dynamics. (b) Temperature profiles showing that fitting this single parameter accurately reproduces the observed data

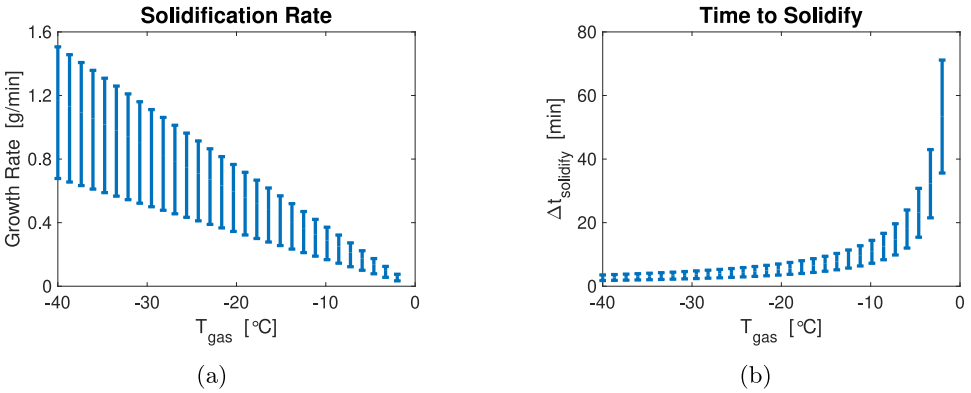

Fig. 15 (a) Ice crystal growth rates that are easily accessible with this chamber. (b) Time required to fully solidify 3 mL of solution for a range of constant gas temperatures

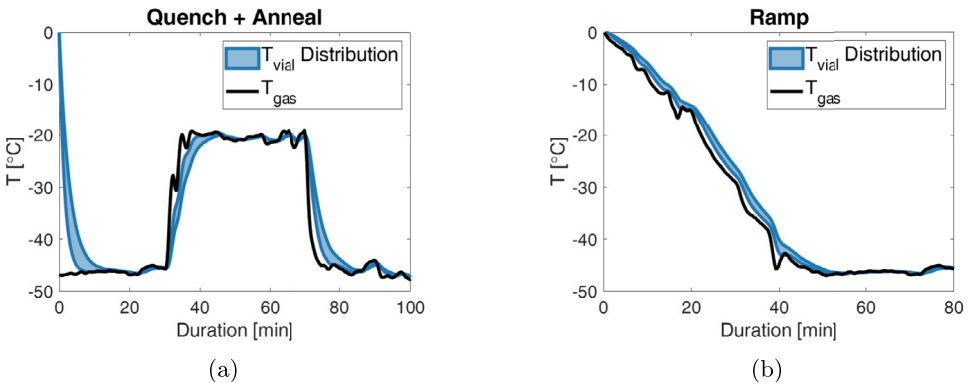

Fig. 16 Inferred vial temperature dynamics in response to measured (a) step and (b) ramp freezing protocols

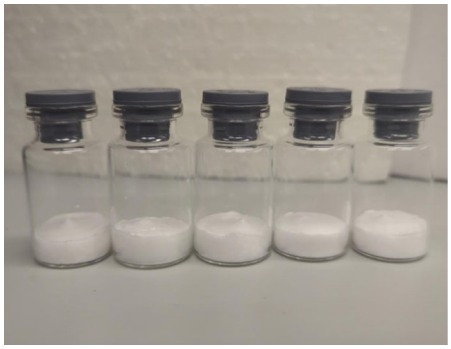

(a)

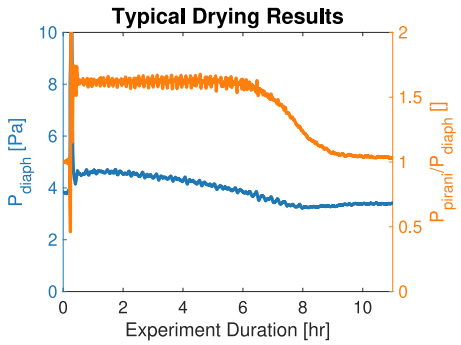

(b)

Fig. 17 (a) Typical cakes produced and (b) detected endpoint of primary drying

Lyophilization Results

Figure 17a shows that the vials lyophilized per the procedure in Section Lyophilization Performance showed no sign of macroscopic collapse. These vials completed primary drying in about nine hours, as reported by the pressure ratio test in Fig. 17b. The efficacy of this drying is reinforced by Karl Fisher titration, which showed that all vials had a residual moisture < 2.5 wt%. These results demonstrate that the excellent uniformity and control of forced convective freezing enables rapid drying of all vials while also enabling continuous processing.

Conclusion

This work describes the design and testing of a forced convection gas freezing chamber for continuous lyophilization. Simulation work screened the initial parameter space to narrow the design scope and provided targets for the physical prototype to meet its functional requirements. The freezing chamber includes a gas recirculation system for efficiency and stability, and it was demonstrated to provide sufficiently uniform gas temperature and flow conditions to vials across its inlets.

The gas temperature in this freezing chamber can rapidly change to match freezing recipes from traditional batch lyophilizers and to access more flexible protocols. Throughout the freezing process, uniformity across all vials in the chamber was maintained within 3°C during dynamic regimes and 0.5°C during steady states. Vials in this chamber could be brought from ambient to slightly subcooled conditions in less than 30 min. After subcooling, a novel method for controlled nucleation was tested which induced nucleation in all vials within 30 s and 1°C. After nucleation, the system has excellent control over the solidification rates within the vials and their post-solidification behavior. Additionally, vials frozen by this method tolerated a rapid primary drying rate, achieving a total drying time of 12 h without collapse and low residual moisture. These results demonstrate the ability of this chamber to freeze vials uniformly and optimally, enabling accelerated drying in a topology compatible with continuous manufacturing.

Supplementary Information

ESM01.mp4: Video from which the frames in Fig. 13 were extracted. The nucleation impulse begins 5 s into the video.

Appendix A: Additional Simulated Geometries

In addition to the loose hexagonal grid presented in Fig. 1a, the initial set of simulations included the simple 3×3 grid geometry shown in Fig. 18a. This geometry simplifies the tray design, but it also occludes more vials from direct cooling gas flow. Simulations were also run where cold gas was fed through the top of the system and exhausted through the sides, as shown in Fig. 18b. This configuration generally had slower conditioning times because less gas impinged directly onto vials. A summary of evaluating both geometries and flow directions is shown in Table 1. These results led to the selection of the loose hexagonal grid with cross-flow for physical prototyping.

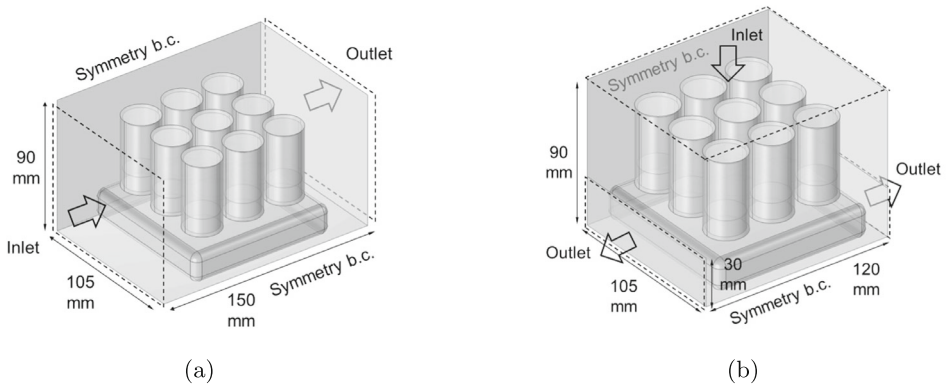

Fig. 18 An alternative (a) vial layout and (b) flow configuration screened in this study

Table 1 The initial simulation results were used to select the hexagonal grid with the left-right flow configuration as the target geometry in this study

Layout	Flow Direction	min(t_{cond}) (min)	max(t_{cond}) (min)
Simple Grid	Left-Right	45	77
Simple Grid	Top-Down	57	88
Hexagonal Grid	Left-Right	43	75
Hexagonal Grid	Top-Down	50	75

Appendix B: Major Hardware Iterations

While the internal geometry of the freezing chamber was determined by the size of the Planar Motors flyway and the simulations for the inlet and outlet positions, the gas flow system underwent the series of iterations shown in Fig. 19 to consistently generate the desired gas flow and temperature conditions.

The first physical prototype (Fig. 19A) used a direct cross-flow approach with no recycle. It was quickly evident that such a strategy wasted too much energy to be feasible, so an initial recycle system was made primarily from cardboard sonotubes (Fig. 19B). This recycle structure proved effective, so an updated recycle structure made from laser cut acrylic plates was constructed to improve assembly and sealing at its interfaces (Fig. 19C). This structure was made entirely from assembled plates, so it included turning vanes to reduce flow losses at its corners. However, the toothed interfaces did not seal sufficiently well. Thus, the acrylic plates defining the recycle shape were made with rounded corners, and a thin acrylic sheet was attached along their outer edges with acrylic weld (Fig. 19D). This design sealed well, but the thin acrylic sheet became brittle at cryogenic temperatures and fractured when subjected to pressure fluctuations. The acrylic was then replaced with stainless steel using the same side plate and thin sheet structure with welded edges (Fig. 19E). This structure generally performed well, but the use of multiple bends in constructing the recirculation duct panels made it more difficult to ensure the bends were done at the correct locations, and the diffuser included extra volume that could contribute to flow losses. The final geometry uses only two bends and a diffuser geometry more conformal to the fans positioned inside it (Fig. 19F). This final structure is also made from aluminum to match the chamber material, avoiding differential thermal expansion stress that could create leaks.

Appendix C: Temperature Control System

As described in Section Gas Temperature Control, this freezing chamber uses a cascade controller to stabilize the temperature of the cooling gas. A piping and instrumentation diagram (P&ID) of the implemented cascade strategy is shown in Fig. 20a. This strategy was necessary because the cryogenic temperatures cause significant thermal contraction of the control valve, leading to inconsistent valve behavior.

Direct control of the valve based on the measured temperature is infeasible because the temperature change timescale, $\mathcal{O}(2\,\text{min})$, is comparable to the process timescale, $\mathcal{O}(10\,\text{min})$, and the valve positioning is very inconsistent. Figure 20b shows the path dependence of the measured flow rate when opening and closing the valve. In particular, the valve gets stuck shut, leading to a large deadband region during opening without any response, followed by a region with an unexpectedly large gain once the valve begins to move.

The cascade controller utilizes the relatively fast outlet flow rate timescale, $\mathcal{O}(5\,\text{sec})$, to correct for the current valve behavior. Although flow rates are generally measured upstream of a control valve to avoid entrance length effects, the two-phase boiling liquid nitrogen feed makes this positioning infeasible. Therefore, the flow meter was placed on the outlet of the chamber, as shown in Fig. 20a.

The cascade loop structure alone is not sufficient to mitigate the large valve position hysteresis, so two modifications to a typical cascade control scheme are implemented. First,

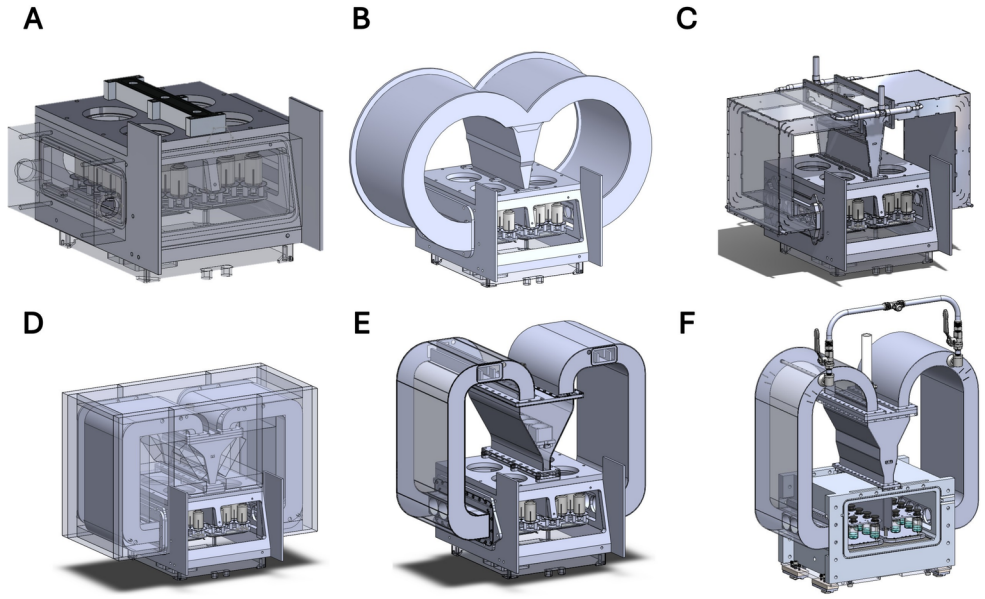

Fig. 19 Refinement of the cooling chamber prototype

a deadband on the valve control signal is implemented to stop actuation of the valve unless the desired control action is larger than 1%. Because the cryogenic temperatures cause the valve to stick, many small actuations lead to no physical movement of the valve. Thus, larger actions must be built up and executed. Second, when the valve needs to open, it is opened a large amount (10%) and then closed to the desired position to avoid the unreliability of the valve opening behavior. After any control action is taken by the valve, the flow rate data for the next 10 s is ignored to avoid being biased by a pressure hammer from the two-phase flow.

This control system was implemented on a CLICK PLC (Automation Direct) running at a typical scan time of 50 ms. An exponentially weighted moving average filter was applied to both the raw temperature and flow rate data with filter timescales of 20 and 40 s respectively. The PID loop period was set to 1 s and all control variables were logged with MATLAB every 10 s. When enabled, this controller can stabilize both the inner flow rate controller (Fig. 21a) and the outer temperature control loop (Fig. 21b).

Appendix D: Estimating Vial Dynamics

D.1 Fitting Per-Vial Heat Transfer Coefficients

During the conditioning experiments presented in Section Conditioning, both the temperature of the liquid water in the vials and the cooling gas temperature were measured as a function of time. These temperatures are coupled through

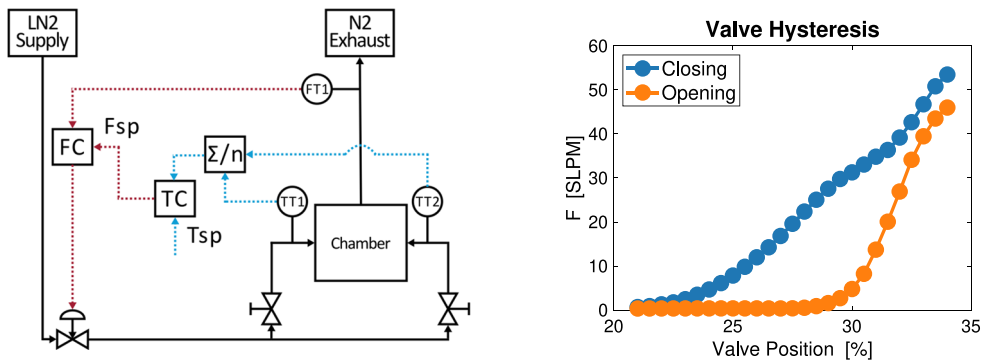

Fig. 20 (a) P&ID diagram for the control system for the gas temperature. (b) Hysteresis measured for the control valve

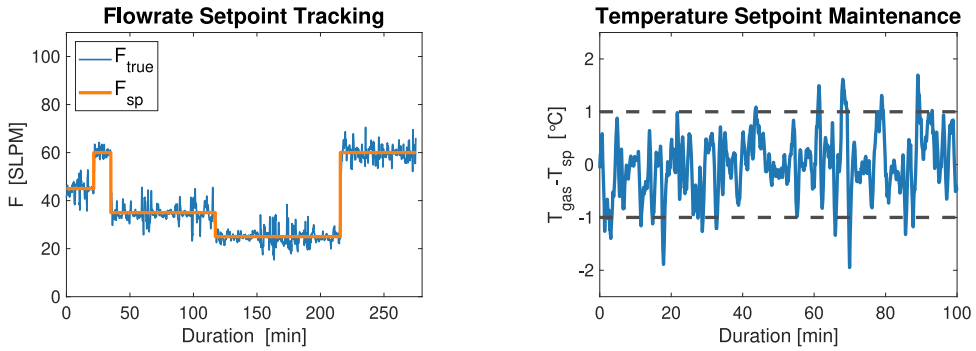

Fig. 21 (a) The inner loop of the cascade controller stabilizes the outlet gas flow rate over a range of setpoints. (b) The fast inner loop enables the chamber to maintain the gas temperature within 1°C of the setpoint over long periods of time

simple convective heat transfer between the gas and the vial. Both the glass vial and the water inside can be treated as lumped material with an average temperature that was measured during the experiment,

$$\frac{\mathrm{d}T_{\mathrm{vial}}}{\mathrm{d}t} = \frac{hA_{\mathrm{vial}}}{m_{\mathrm{solution}}C_{p,\mathrm{solution}} + m_{\mathrm{vial}}C_{p,\mathrm{vial}}}\left(T_{\mathrm{vial}} - T_{\mathrm{gas}}\right) \tag{D1}$$

The surface area of the vial, A, was calculated by approximating the 10R vial as a cylinder with a 12 mm radius and a 30 mm height. The mass of each vial was estimated as 9.2 g after measuring the average mass of 50 vials. The mass of solution in each vial was estimated as 3 g based on the nominal fill volume. The heat capacity of the solution and glass were approximated using the values for pure water and silica glass.

Two strategies could be used to fit h: (1) explicitly calculate $\frac{\mathrm{d}T_{\mathrm{vial}}}{\mathrm{d}t}$ using a finite difference approximation at each point, or (2) use an ode solver like `ode45` and pass h and the true gas temperature to it. If (1) is used, a best-fit h can be calculated directly from matrix inversion because right hand side is linear in h. If (2) is used, an optimization can be run over h (e.g. using `lsqnonlin`) which minimizes the square error between the fit and true T_{vial} trajectories. Option (2) was selected for this work to avoid poor conditioning of the large system of equations created by (1). The call to `ode45` restricted the maximum step size of the function to be less than 5 times the average sampling period of the T_{gas} data. This limitation prevents the solver from jumping past any fast dynamics that occurred.

Critically, while lumped analysis only tracks the evolution of the liquid solution and glass vial control volume, it determines a heat transfer coefficient h that only depends on the geometry. Therefore, the evolution of the freezing (and frozen) water can be inferred by using the appropriate thermodynamic properties because the geometry stays constant.

D.2 Applying Per-Vial Heat Transfer Coefficients

The results in Section Induced Nucleation show empirically that nucleation can be induced in all vials nearly simultaneously without significant cooling. After this nucleation event occurs, the sub-cooled solution in the vial rapidly forms ice crystals as the solution jumps back to the equilibrium freezing temperature. An energy balance around the solution shows that during this rapid, $\mathcal{O}(1\ \mathrm{sec})$ impulse, the initial mass of frozen solution is:

$$m_{\mathrm{frozen}}(t_0) = \frac{m_{\mathrm{solution}}C_p\Delta T_{\mathrm{subcool}}}{\Delta H_{\mathrm{fusion}}} \tag{D2}$$

After nucleation occurs, all of the heat removed from the cooling vial and solution assembly is sunk into the solidifying solution. This process continues until $m_{\mathrm{frozen}} = m_{\mathrm{solution}}$ and follows the simple ODE:

$$\frac{\mathrm{d}m_{\mathrm{frozen}}}{\mathrm{d}t} = \frac{hA_{\mathrm{vial}}}{\Delta H_{\mathrm{fusion}}}\left(T_{\mathrm{vial}} - T_{\mathrm{gas}}\right) \tag{D3}$$

For simplicity, this work assumes that during solidification $T_{\mathrm{vial}} = T_{\mathrm{freeze}} = 0°\mathrm{C}$. After solidification completes, the vial and frozen solution will begin to cool in the presence of cold gas as described by the energy balance around the vial:

$$\frac{\mathrm{d}T_{\mathrm{vial}}}{\mathrm{d}t} = \frac{hA_{\mathrm{vial}}}{m_{\mathrm{solution}}C_{p,\mathrm{ice}} + m_{\mathrm{vial}}C_{p,\mathrm{vial}}}\left(T_{\mathrm{vial}} - T_{\mathrm{gas}}\right) \tag{D4}$$

The only difference between Eqs. D1 and D4 is the replacement of the properties of liquid water with those of ice.

Supplementary Information The online version contains supplementary material available at https://doi.org/10.1007/s12247-025-10037-0.

Acknowledgements This work was supported by the Food and Drug Administration under Grant FD006755-02. The cooling chamber and recirculation ductwork used for the freezing experiments was manufactured by Josh Dittrich at StartSomething in Somerville, MA who also provided helpful machineability feedback. Planar Motors Inc. provided helpful information to operate their magnetic levitation system at cryogenic temperatures and to incorporate the flyway into the freezing chambers. The vials used in this study were provided by Soffieria Bertolini.

Author Contributions Conceptualization: A.H.S., B.L.T., R.D.B., R.P. Formal analysis: L.S., R.P.K. Funding acquisition: A.H.S., B.L.T., R.D.B. Investigation: L.S., R.P.K., S.J.B. Methodology: L.S., R.P.K., S.J.B. Resources: A.H.S., B.L.T., R.D.B., R.P. Software: L.S., R.P.K. Supervision: A.H.S., B.L.T., R.D.B., R.P.

Funding 'Open Access funding provided by the MIT Libraries'.

Data Availability No datasets were generated or analysed during the current study.

Declarations

Conflict of Interest The authors declare that they have no known conflict of interest or personal relationships that could have appeared to influence the work reported in this paper.

References

1. Rey L, (ed.). Freeze-drying/lyophilization of pharmaceutical and biological products 3 edn. Boca Raton, Florida: CRC Press; 2016. https://www.taylorfrancis.com/books/9781439825761.
2. Gan KH, Bruttini R, Crosser OK, Liapis AI. Heating Policies during the primary and secondary drying stages of the lyophilization process in vials: effects of the arrangement of vials in clusters of square and hexagonal arrays on trays. Dry Technol. 2004;22:1539–75. http://www.tandfonline.com/doi/abs/10.1081/DRT-200025596.
3. Pisano R, Arsiccio A, Capozzi LC, Trout BL. Achieving continuous manufacturing in lyophilization: technologies and approaches. Eur J Pharm Biopharm. 2019;142:265–79. https://linkinghub.elsevier.com/retrieve/pii/S0939641119303261.
4. Capozzi LC, Trout BL, Pisano R. From batch to continuous: freeze-drying of suspended vials for pharmaceuticals in unit-doses. Ind Eng Chem Res. 2019;58:1635–49. https://pubs.acs.org/doi/10.1021/acs.iecr.8b02886.
5. Horn J, Friess W. Detection of collapse and crystallization of saccharide, protein, and mannitol formulations by optical fibers in lyophilization. Front Chem. 2018;6:4. http://journal.frontiersin.org/article/10.3389/fchem.2018.00004/full.
6. Johnson RE, Kirchhoff CF, Gaud HT. Mannitol-sucrose mixtures-versatile formulations for protein lyophilization. J Pharm Sci. 2002;91:914–22. https://linkinghub.elsevier.com/retrieve/pii/S0022354916309777.
7. Velardi SA, Barresi AA. Development of simplified models for the freeze-drying process and investigation of the optimal operating conditions. Chem Eng Res Des. 2008;86:9–22. https://linkinghub.elsevier.com/retrieve/pii/S0263876207000123.
8. Arsiccio A, Pisano R. The ice-water interface and protein stability: a review. J Pharm Sci. 2020;109:2116–30. https://linkinghub.elsevier.com/retrieve/pii/S0022354920301817.
9. Strambini G, Gabellieri E. Proteins in frozen solutions: evidence of ice-induced partial unfolding. Biophys J. 1996;70:971–6. https://linkinghub.elsevier.com/retrieve/pii/S0006349596796406.
10. Oddone I, Barresi AA, Pisano R. Influence of controlled ice nucleation on the freeze-drying of pharmaceutical products: the secondary drying step. Int J Pharm. 2017;524:134–40. https://linkinghub.elsevier.com/retrieve/pii/S0378517317302648.
11. Searles JA, Carpenter JF, Randolph TW. The ice nucleation temperature determines the primary drying rate of lyophilization for samples frozen on a temperature-controlled shelf. J Pharm Sci. 2001;90:860–71. https://linkinghub.elsevier.com/retrieve/pii/S0022354916307675.
12. Colucci D, Fissore D, Barresi AA, Braatz RD. A new mathematical model for monitoring the temporal evolution of the ice crystal size distribution during freezing in pharmaceutical solutions. Eur J Pharm Biopharm. 2020;148:148–59. https://linkinghub.elsevier.com/retrieve/pii/S0939641120300084.
13. Deck L-T, Mazzotti M. Characterizing and measuring the ice nucleation kinetics of aqueous solutions in vials. Chem Eng Sci. 2023;272:118531. https://linkinghub.elsevier.com/retrieve/pii/S0009250923000878.
14. Patel SM, Bhugra C, Pikal MJ. Reduced pressure ice fog technique for controlled ice nucleation during freeze-drying. AAPS PharmSciTech. 2009;10:1406. http://link.springer.com/10.1208/s12249-009-9338-7.
15. Oddone I, Pisano R, Bullich R, Stewart P. Vacuum-induced nucleation as a method for freeze-drying cycle optimization. Ind Eng Chem Res. 2014;53:18236–44. https://pubs.acs.org/doi/10.1021/ie502420f.
16. Searles JA, Carpenter JF, Randolph TW. Annealing to optimize the primary drying rate, reduce freezing-induced drying rate heterogeneity, and determine T'g in pharmaceutical lyophilization. J Pharm Sci. 2001;90:872–87. https://linkinghub.elsevier.com/retrieve/pii/S0022354916307808.
17. Hawe A, Fries W. Impact of freezing procedure and annealing on the physico-chemical properties and the formation of mannitol hydrate in mannitol-sucrose-NaCl formulations. Eur J Pharm Biopharm. 2006;64:316–25. https://linkinghub.elsevier.com/retrieve/pii/S0939641106001500.
18. Rambhatla S, Tchessalov S, Pikal MJ. Heat and mass transfer scale-up issues during freeze-drying, III: control and characterization of dryer differences via operational qualification tests. AAPS PharmSciTech. 2006;7:E61–70. http://link.springer.com/10.1208/pt070239.
19. Lammens J, et al. Spin freezing and its impact on pore size, tortuosity and solid state. Pharmaceutics. 2021;13:2126. https://www.mdpi.com/1999-4923/13/12/2126.
20. D'Imprima E, et al. Protein denaturation at the air-water interface and how to prevent it. eLife. 2019;8:e42747. https://elifesciences.org/articles/42747.

21. Colombié S, Gaunand A, Lindet B. Lysozyme inactivation under mechanical stirring: effect of physical and molecular interfaces. Enzym Microb Technol. 2001;28:820–6. https://linkinghub.elsevier.com/retrieve/pii/S0141022901003404.
22. Samantray S, Cheung DL. Effect of the air-water interface on the conformation of amyloid beta. Biointerphases. 2020;15:061011. https://pubs.aip.org/bip/article/15/6/061011/1079469/Effect-of-the-air-water-interface-on-the.
23. Schaal Z, et al. Optimization of continuous spin-freeze-drying: the role of spin-freezing on quality attributes and drying efficiency of a model peptide formulation. Eur J Pharm Sci. 2025;204:106963. https://linkinghub.elsevier.com/retrieve/pii/S0928098724002768.
24. Dempsey P, Bansal P. The art of air blast freezing: design and efficiency considerations. Appl Therm Eng. 2012;41:71–83.
25. Flores R. Material handling for continuous lyophilization process. Master's thesis, Massachusetts Institute of Technology, Cambridge Massachusetts; 2022.
26. Pisano R. Automatic control of a freeze-drying process: detection of the end point of primary drying. Dry Technol. 2022;40:140–57. https://www.tandfonline.com/doi/full/10.1080/07373937.2020.1774891.

Authors and Affiliations

Steven J. Burcat[1] · Rohan P. Kadambi[2] · Lorenzo Stratta[3] · Richard D. Braatz[2] · Roberto Pisano[3] · Alexander H. Slocum[1] · Bernhardt L. Trout[2]

✉ Bernhardt L. Trout
trout@mit.edu

Steven J. Burcat
sburcat@mit.edu

Rohan P. Kadambi
kadambi@mit.edu

Lorenzo Stratta
lorenzo.stratta@outlook.com

Richard D. Braatz
braatz@mit.edu

Roberto Pisano
roberto.pisano@polito.it

Alexander H. Slocum
slocum@mit.edu

[1] Department of Mechanical Engineering, Massachusetts Institute of Technology, Cambridge, MA, USA

[2] Department of Chemical Engineering, Massachusetts Institute of Technology, Cambridge, MA, USA

[3] Department of Applied Science and Technology, Politecnico di Torino, Turin, Italy